Experimental and Numerical Pore Scale Study of Residual Gas Saturation in Water/Gas Imbibition Phenomena

Hekmatzadeh, Mahnaz •

1. Chemical Engineering Department, Amirkabr University of Technology, P.O. Box 158754413 Tehran, I.R. IRAN
2. IOR Research Institute, National Iranian Oil Company, P.O. Box 1969813771 Tehran, I.R. IRAN

Dadvar, Mitra* +

Chemical Engineering Department, Amirkabr University of Technology, P.O. Box 158754413 Tehran, I.R. IRAN

Emadi, Mohammad Ali

IOR Research Institute, National Iranian Oil Company, P.O. Box 1969813771 Tehran, I.R. IRAN

ABSTRACT: *Residual gas saturation is one of the most important parameter in determining recovery factor of water-drive gas reservoir. Visual observation of processes occurring at the pore level in micromodels can give an insight to fluid displacements at the larger scale and also help the interpretation of production performance at reservoir scale. In this study experimental tests in a glass micromodel were used to determine the influence of the capillary number and pore morphology on the residual gas saturation in gas–liquid two-phase flow. The saturation of the phases was determined through recorded images in the micromodel. 2D modeling and simulation of this process is presented in this study and simulation results are verified by comparing to experimental results where sufficient agreement was confirmed. The simulation results indicate that pore morphology and capillary number have significant influence on the competition between frontal displacement and snap-off. Frontal displacement leads to high recovery and snap off causes gas entrapment. It is concluded that increasing the pore and throat sizes, increasing the coordination number and increasing angularity (decreasing half angle) result in reducing the residual gas amount. The results also indicate that residual gas saturation is not only a function of petrophysical property and pore morphology, but also it depends on flow rate and the experimental procedure. Residual gas saturation does not change significantly when N_c is less than 10^{-7}.*

KEY WORDS: *Micromodel; Residual gas; Pore network model; Film flow; Imbibition; Snap-off.*

INTRODUCTION

During production from water drive gas reservoirs, water imbibition into the reservoir leads trapping some gas as Residual Gas Saturation (RGS) behind the water gas contact zone. Experimental studies in core scale show

* *To whom correspondence should be addressed.*
+ *E-mail: dadvar@aut.ac.ir*
1021-9986/15/3/109 *12/$/3.20*

that RGS varies between 15 and 80% [1]. RGS influences the economics of gas reservoir development, especially in heterogeneous reservoirs. Due to the high importance of spontaneous imbibition on hydrocarbon recovery it has been the subject of many studies, however, most of these studies focus on residual saturation in oil/water systems and there are very limited studies in gas/water flow. Some studies conducted experimental core analysis measurements to investigate gas entrapment. *Land* (1971) proposed a relationship between the trapped gas saturation and the initial gas saturation based upon experimental data for consolidated media [2]. Other studies have questioned the validity of applying Land's trapping relationship to various rock/fluid systems [3, 4].

Many studies have tried to correlate trapped gas saturation to reservoir petrophysical properties. *Chierici et al.* (1963) failed to correlate RGS values with porosity, permeability or irreducible water saturation for samples with different lithology types [5]. *Katz* (1966) presented a very general relationship between gas saturation and porosity on sand and sandstone cores, but he did not find any trend against permeability [6]. *MacKay* (1974) reported a very weak relationship between porosity and RGS [7]. *Delclaud* (1991) observed wide variations of RGS for the sandstone cores in North Sea gas field [8].

The effect of water flooding rates on RGS is also investigated. Several authors demonstrated that RGS in water flooding and spontaneous imbibition are very close [1, 8, 9]. *Although Bull et al.* (2011) observed that RGS in sandstones depends on imbibition rate [10].

This short review shows no unique trends in the experimental results, since the trapped saturation depends on the details of the pore structure and also the experimental procedure. However, the role of petrophysical properties that influence capillary trapping is still a challenging subject.

Another approach for investigating trapped saturation is pore-scale modelling. However, uncertainties in wetting films displacement mechanism impose difficulties in evaluating trapped gas modelling. *Lenormand* (1999) is the first person who studied basic displacement mechanisms in air/water displacement in micromodels [11]. He observed that imbibition displacement events, frontal displacement and snap-off, and showed that the competition between these two events depends on the pore space geometry and flow rate. Thus, residual saturation depends on the percentage of frontal and snap-off events.

Blunt & Scher (1995) developed a dynamic 3D pore network model of two-phase flow of oil-water. To estimate the film pressure of an occupied element, they assumed an effective path length from the network inlet to the occupied element. Thus, the dynamic nature of film swelling in snap-off event is not included [12].

Mogensen & Stenby (1998) also developed a 3D dynamic pore network model using the simplifying assumption of constant conductance of wetting fluid in corner films throughout the displacement that is clearly an unrealistic assumption [13]. *Hughes & Blunt* (2000) proposed a simpler model to compute the competition between snap-off and frontal displacements, but the wetting phase pressures are calculated periodically rather than calculating them after filling each element with wet fluid [14].

The objective of this research is to use a glass micromodel to observe displacement of gas/water in imbibition process and identify the effect of pore morphology (pore and throat size, pore shape, aspect ratio and coordination number) and capillary number on the RGS. Then a dynamic pore network model is developed to simulate the experiments to check the consistency of the experimental data. The new dynamic pore network model for imbibition can overcome aforementioned difficulties in previous modeling.

All of the previous models studied oil-water displacement, while gas-water displacement is studied here. Also, all of the previous aforementioned models are based on constant film conductivities, however, snap-off occurrence ahead of the displacement front is considered in this study. In our previous study [15], a system of non-linear equations is solved implicitly to update pressure and saturation of each element ahead of the displacement front in a 3D network. But in this study a 2D network model is developed to display the fluid flow mechanism which is observed in the micro model displacement of the gas-water flow. Then an algorithm is developed to match the network parameter with micromodel one. Moreover, in this modeling the pressure is calculated implicitly while saturation terms are calculated explicitly.

The paper is organized as follows. First the important part of the experimental setup, materials and procedures is briefly described. Then pore structure and modelling

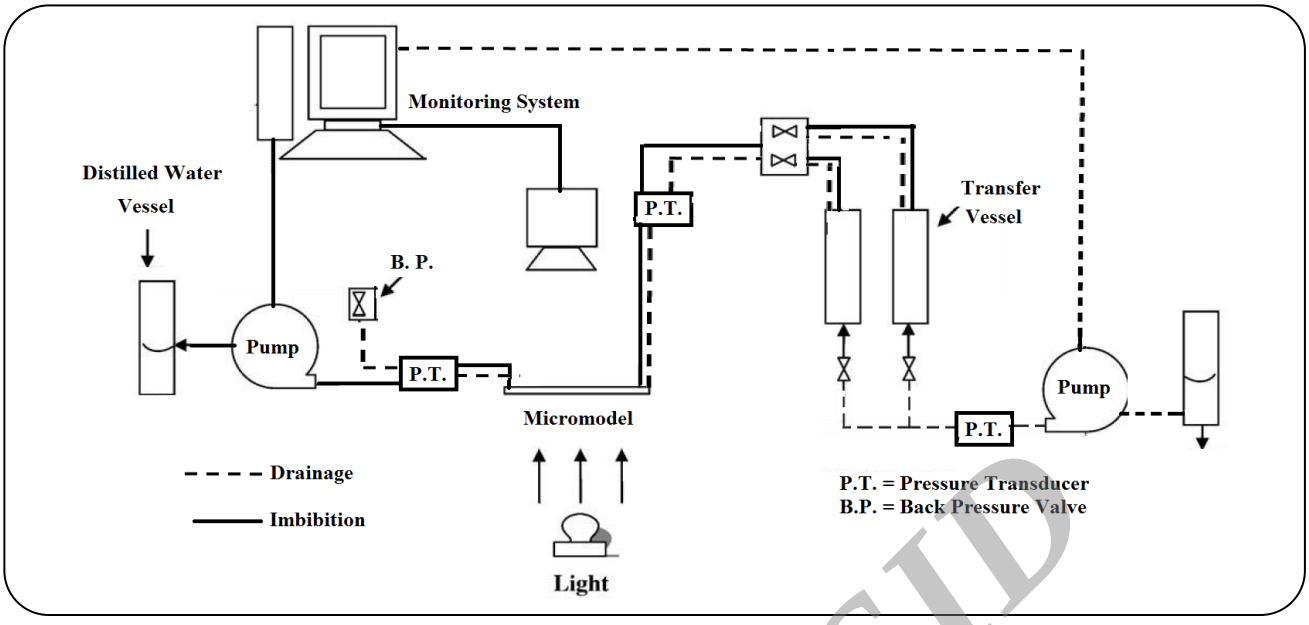

Fig. 1: Micromodel Set-up.

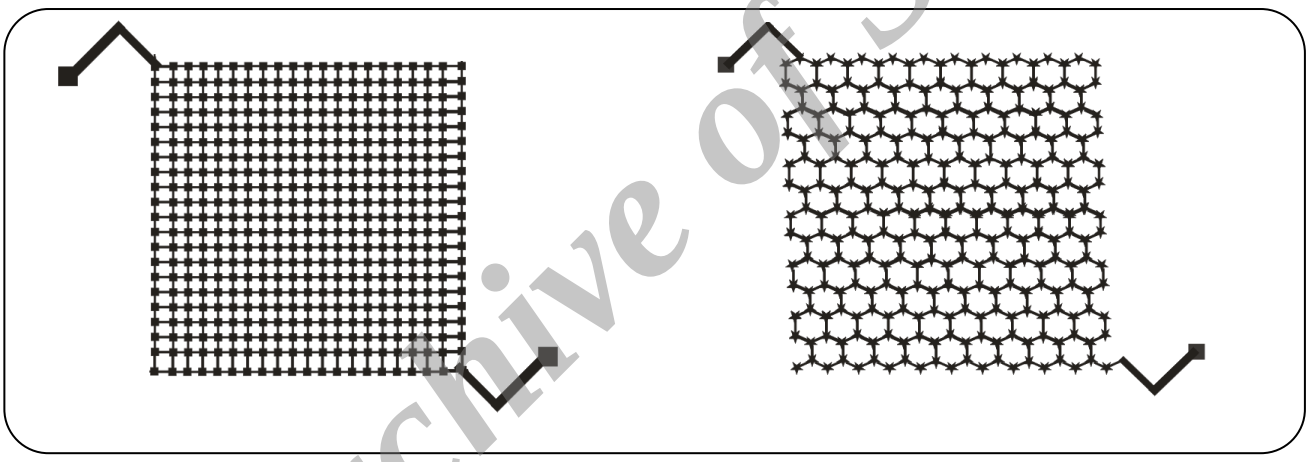

Fig. 2: Micromodel Patterns.

method for imbibition displacement are explained and the simulation procedure is illustrated. Afterwards, modelling results are validated and then compared to micromodel results. The final part includes a summary of the conclusions.

EXPERIMENTAL SECTION

Fig. 1 shows a schematic diagram of the two micromodel set-ups which is designed to study drainage and imbibition displacement in micromodels for investigating RGS in gas reservoirs with an active aquifer. These set-ups consist of a micromodel and its holder, fluid injection section, monitoring system and the computer system.

The micromodels glass plate has approximately 5 cm length, 10 cm width and 0.6cm height, respectively. The micromodel pattern is represented by a 2D pore network model of wide spaces called "pore" that are connected by narrower regions termed as "throats". In this study two 4*4 cm^2 pattern with square and star pore shaped and different pore size distributions are made by using laser technology (Jamieson Laser CMA-1910 TF). The micromodel patterns are shown schematically in Fig. 2.

Table 1 illustrates the structural properties of micromodels. In this table the aspect ratio is the ratio of the pore to throat diameter and coordination number refers to the number of throats that are connected to a pore.

Table 1: Characteristics of micromodels.

No.	1	2	3
Micromodel Size(cm^2)	4×4	4×4	4×4
Pore Size (μm)	650	650	200
Throat size (μm)	280	280	70
Aspect Ratio	2.31	2.71	2.85
Coordination Number	4	4	3
Etched Thickness(μm)	26	21	21
Porosity (%)	30.3	27.5	26.7
Pore Shape	Square	Square	Star-Shaped
Pattern	Fig.2 (a)	Fig.2 (a)	Fig.2 (b)
Abs.Perm.(D)	(1.79±0.12)	(0.93±0.14)	(0.91±0.12)

Table 2: Fluid properties.

Property	Water	Air
Density (g/cm^3)	0.99969	0.000876
Viscosity (Pa.s)	0.9 *10-3	19 * 10-6 Pa.s
Surface Tension (N/m)	76 * 10-3	
Contact angle(deg)	0.0	

Average porosity is calculated by dividing the total pore and throat surface area by micromodel surface area. The absolute permeability of a micromodel is calculated by using Darcy's law with measuring flow rate and pressure drop.

Fluid injection section consists of a positive displacement pump (Bench Floor, Dual Pump series) VINCI Model XU_O that injects fluid into the micromodels with an accuracy of 10^{-5} cc/min. The camera system as a monitoring system is capable of working at a magnification up to 50 times to capture pictures. The computer system is also used for recording pressures, pictures and capturing time. The physical properties of the fluid are listed in Table 2.

The experiments include qualitative observations via digital camera imaging and quantitative investigations based on image analysis. Experiments involve three steps; first saturating the micromodel with water, then displacing the water phase with air (drainage) and finally displacing air with water (imbibition).

After saturating the micromodel with water, drainage experiment is initiated by setting a desired pressure for the experiments. Then constant rate metering pump injects five pore volumes of gas to the micromodel in 10^{-4} cc/min. The gas occupies the center of pores and throats and water that is wet fluid remains in the element's corners. The amount of initial water saturation in different micromodels with different patterns, shape and pore size distribution is completely different. Fig. 3 shows the fluid distribution in a drainage displacement experiment in star cross sections pores.

In imbibition experiment, a water cylinder with the same pressure as micromodel pressure is connected to the micromodel inlet and gas is evacuated from the micromodel outlet at a constant flow rate. Thus, gas pressure is decreased and water invades the porous media simultaneously. Then RGS is determined by image analyzing. The experiment continues until water reaches to the outlet pore of the network and the final RGS is verified. The distribution of the remaining gas phase after free imbibition is shown in Fig. 4 for a pattern star shaped pore cross sections.

THEORITICAL SECTION

Numerical Modelling

In this section pore network structure based on the micromodel patterns and pore size distributions are described. The displacement process and fluid flow equations are also illustrated.

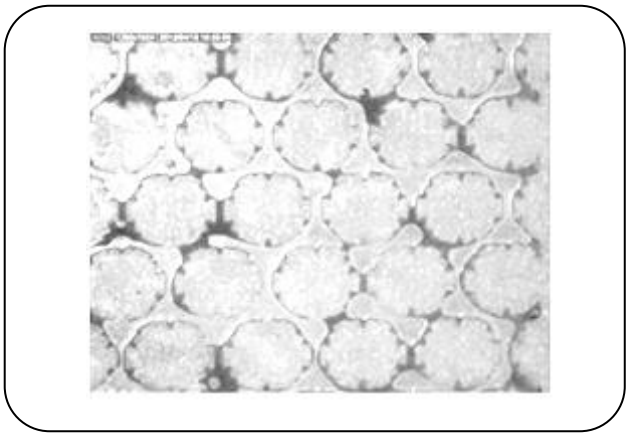

Fig. 3: Fluid distributions after drainage displacement in star shaped cross section.

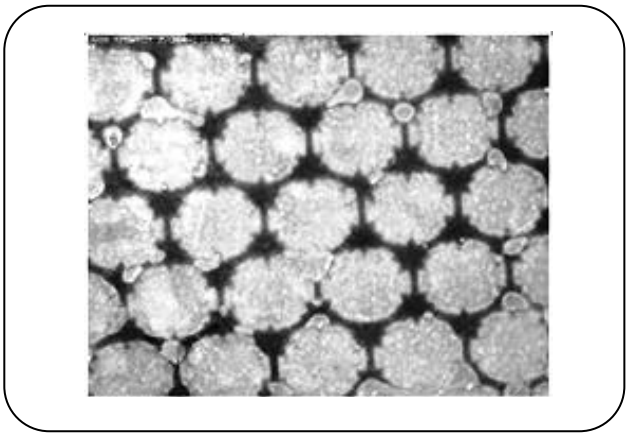

Fig. 4: Fluid distributions after imbibition displacement in star shaped pore cross section.

Pore-network structure

The first step in pore network modelling is to map the pore spaces to a pore network. In this study, the structure or the pore space is selected approximately the same as the micromodel pore size distribution and a 2D pore network with coordination number of four having square-shaped surface area of pores and throats is used as the basic model. Pore inscribed radius (R_p) is generated based on the Weibull distribution [16].

$$R_p = \left(R_{max} - R_{min}\right)\left(-\delta \ln\left[x\left(1-e^{-1/\delta}\right)+e^{-1/\delta}\right]\right)^{1/\gamma} + R_{min} \quad (1)$$

where R_{max} and R_{min} are maximum and minimum radius, respectively and x is a random number. δ and γ are Weibull distribution parameters that in the basic model are chosen to be 0.2 and 0.9, respectively. Throat radii (R_t) are correlated as follows,

$$R_t = \min\left\{R_{p,i}, R_{p,j}, \frac{R_{p,i}+R_{p,j}}{2\,AR}\right\} \quad (2)$$

The aspect ratio, *AR*, is defined as the ratio of inscribed radii of pores and throats and it is set equal to 2.31 in the basic model that is the same as the micromodel No.1 *AR*.

$$AR = \frac{R_p}{R_t} \quad (3)$$

Throat lengths, L_t, are also selected to be equal to 700 μm which is the same as micromodel No.1. Fig. 5 shows pore and throat size distributions.

In this study, pore and throat cross section shape is considered to be square in basic model. To investigate the effect of pore shape on residual saturation the pore cross section shape is changed to star-shaped. The total cross-sectional area, A_t, of the pores in star-shaped cross section is calculated as follows [17],

$$A_t = N\,(\cos(\pi k/N))^2[\tan(\pi k/N) - \tan(\pi(k-1)/N)]R^2 \quad (4)$$

where N is the number of pointed star in a kth point connected star. The cross section area of the wet films, A_w, is [18]

$$A_w = Nr_w^2\left(\cos\theta\left(\cot\alpha\cos\theta-\sin\theta\right)+\theta+\alpha-\frac{\pi}{2}\right) \quad (5)$$

where θ is contact angle and α is the corner's half angle that for the star-shaped is calculated as follows [17],

$$\alpha = \pi\left(\frac{N-2k}{N}\right) \quad (6)$$

in Eq. (5) r_w is curvature radii of wet films in the corners that relates to interfacial tension, σ, and local capillary pressure, P_c, by the Young-Laplace equation,

$$r_w = \frac{\sigma}{P_c} = \frac{\sigma}{P_{nw}-P_w} \quad (7)$$

The wetting fluid saturation in an element, S_w, is equal to the fraction of cross-section area occupied by the wetting fluid that is:

$$S_w = \frac{A_w}{A_t} \quad (8)$$

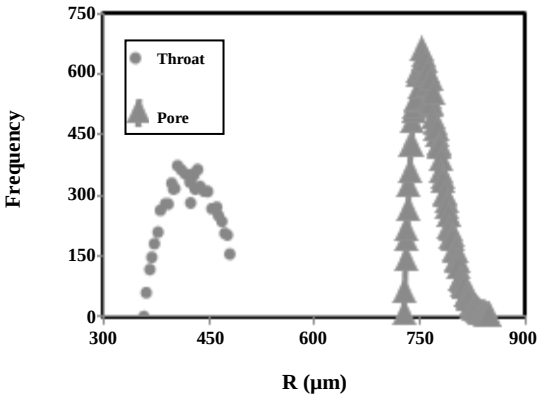

Fig. 5: Pore and throat size distributions.

Displacement Process Modeling

Two types of displacements, snap off and frontal displacement, are considered in water imbibition modelling. The pore network's initial and boundary conditions for this process are similar to micromodel experiments. The network's inlet is connected to a constant pressure wetting fluid source and a constant flow rate of non-wetting fluid is considered at the outlet as a sink. In transverse directions, no flow boundary conditions are assumed.

For the modelling of fluid flow in the pore network model viscous forces in bulk fluids (fluid occupying the centres of the pores and throats) are negligible. This is a reasonable assumption for capillary numbers less than 10^{-3}–10^{-4} [19] which covers a wide range of capillary numbers normally encountered in reservoir displacements and laboratory tests.

The three possible flow mechanisms in pore scale imbibition are frontal displacement or piston-type invasion in throats at the front face, snap-off or invasion in throats ahead of the front face by capillary driven swelling that causes eventual rupture of corner films and frontal displacement in pores [20-22].

In frontal displacement a throat completely fills by the invading wetting phase. The threshold pressure in this mechanism is calculated by [23]

$$P_{c,t} = \frac{\delta}{R_t}\left\{\cos\theta + \sqrt{\frac{\tan\alpha}{2}\left[\sin(2\theta) + \pi - 2(\alpha+\theta)\right]}\right\} \quad (9)$$

Snap-off displacement in a throat is the invasion of wetting-phase arc menisci that is present in its corners. The snap-off threshold capillary pressure, $P_{c,thS}$, is [23]

$$P_{c,thS} = \frac{\delta(\cos\theta - 2\sin\theta)}{2R_t \cot\alpha} \quad (10)$$

Snap-off in a throat causes creation of two piston-type interfaces and increases throat capillary pressure from $P_{c,thS}$ to throat frontal displacement threshold capillary pressure of $P_{c,t}$, that is given in Eq. (9). The local reduction in wetting fluid pressure makes the wetting fluid flow into the throat and the new piston type interfaces retract to the adjoining pores.

The third displacement mechanism in imbibition is piston type filling of pores. It depends on the pore's size and the number of connected throats filled with non-wet fluid. There exists Z_j-1 of such events, for a pore with coordination number of Z_j, that are referred as I_1 to $I_{Zj\text{-}1}$. There are several empirical correlations for calculating pore's threshold capillary pressure, $P_{c,n}$, in the piston-type displacement event. The following equations are used to calculate $P_{c,n}$ in this study [23, 24];

$$P_{c,n} = \frac{1}{n}\frac{2\sigma\cos\theta}{R_p} \quad (11)$$

If the local capillary pressure of an element is less than the element's threshold capillary pressure, one of the imbibition displacement events occur. To find out which of the above mechanisms occur in the connected elements to the front, wetting film pressures have to be calculated in them.

For the initiating of imbibition process at constant gas flow rate, the pressure of the non-wet fluid at the outlet pore of the network is determined by using the network's equivalent conductance in pores and throats[13],

$$g_{nw,i} = \frac{\pi r_e^4}{8\mu_{nw} l} \quad (12)$$

$$r_e = 0.5*\left(\sqrt{\frac{A_{nw}}{\pi}} + R\right) \quad (13)$$

Since pressure gradient in the non-wet fluid is neglected, P_{nw}, is constant throughout the displacement and is equal to the calculated pressure at the network outlet

$$\sum g_{ij}(P_{nw,i} - P_{nw,j}) = q_{g,out} \quad (14)$$

The pressure gradient in wetting fluid is also neglected in this study and the water pressure from

the inlet pore to the displacement front is equal to the inlet pressure.

The wetting film flow rate from element *i* to a neighbour element *j* is

$$q_{w,ij} = g_{ij}(P_{w,i} - P_{w,j}) \quad (15)$$

Where $P_{w,i}$ and $P_{w,j}$ are wet fluid pressures at elements *i* and *j*, respectively and g_{ij} is the effective film conductance of the wetting fluid flow in between elements *i* and *j* that is determined by the harmonic mean of the films conductance of that elements[14],

$$\frac{1}{g_{ij}} = \frac{1}{g_i} + \frac{1}{g_j} \quad (16)$$

The conductance of a corner film is given by [25]

$$g_i = \frac{A_w r_w}{\beta \mu_w L_i} \quad (17)$$

Where β is the dimensionless flow resistance proposed by *Ransohoff & Radke* (1988), μ_w is wetting fluid viscosity and L_i is pore or throat length. The expression for β is developed by *Zhou et al.* (1997) for no-slip boundary condition at solid-fluid interface and free-slip boundary condition at fluid-fluid interface [26],

$$\beta = \frac{12 \sin^2\alpha (1-B)^2 \Psi_3^2}{(1-\sin\alpha)^2 B^2 (\Psi_1 - B\Psi_2)^2} \quad (18)$$

Where

$$\Psi_1 = \cos^2(\alpha+\theta) + \cos(\alpha+\theta)\sin(\alpha+\theta)\tan\alpha, \quad (19)$$

$$\Psi_2 = 1 - \frac{\theta}{\left(\frac{\pi}{2}-\alpha\right)}, \quad (20)$$

$$\Psi_3 = \frac{\cos(\alpha+\theta)}{\cos\alpha}, \quad (21)$$

$$B = \left(\frac{\pi}{2}-\alpha\right)\tan\alpha \quad (22)$$

For computing wetting film pressures at pores and throats in other time steps, continuity equation for the wetting fluid is used as follows:

$$\sum_{Z_i} q_{w,ij} + \frac{\partial V_{w,i}}{\partial t} = 0 \quad (23)$$

where $V_{w,i}$ is water film volume in element i. The summation is over the elements connected to element i. Substituting Eq. (19) into Eq. (27) gives

$$\sum_{Z_i} g_{ij}\left[P_{w,i} - P_{w,j}\right] = V_i \frac{\partial S_{w,i}}{\partial t} \quad (24)$$

where V_i is the volume of element i and $S_{w,i}$ is the corresponding wetting fluid saturation. Eq. (28) should be used for all elements to update wetting fluid film pressure and saturation in them. This is accomplished by using an explicit finite-difference scheme as follows:

$$\sum_{Z_i} g_{ij}\left[P_{w,i}^{n+1} - P_{w,j}^{n+1}\right] = V_i \frac{S_{w,i}^{n+1} - S_{w,i}^{n}}{\Delta t} \quad (25)$$

where Δt is time interval and superscripts n and n+1 refer to time steps. The time interval is determined based on the filling time of the element with maximum threshold capillary pressure of the wetting fluid that has minimum filling time within the network elements and satisfies the stability criteria.

$$\Delta t = \frac{V_i (1 - S_{w,i}^{n})}{Q_{i,w}} \quad (26)$$

where $Q_{i,w}$ denotes accumulation rate of the wetting fluid in element i, that is:

$$Q_{i,w} = \sum_{Z_i} q_{w,ij}^{n} \quad (27)$$

Simulation

The simulation data for the fluid properties and network structure are presented in Table 2 and Fig. 5, respectively. The simulation procedure of dynamic pore scale imbibition is as follow. A FORTRAN program is developed and used for a 40×40 pore network.

1- Match the permeability and porosity of the network model with the micromodel; to do this a pressure calculation is performed and the total flow rate, permeability and porosity is calculated. Pore radii are scaled until the agreement between calculated and micromodel set-point values are close enough.

2- Determine the radius of curvature between the wet and non-wet fluids; an initial guess for $r_{w/nw}=r/2$ is used in all the elements. Then the following parameters are calculated: cross section area by Eq. (5), conductance

by Eqs. (20), (21) and wetting fluid film pressure by Eq. (29) for all the corners. After that Eq. (7) is used to update the radius of curvature based on the calculated wet pressure until convergence is reached.

3- When the crevice curvatures are calculated, displacement simulation starts. The pore network is initially filled with non-wetting phase in the center of the elements and wetting phase residing in the corners.

4- The global capillary pressure is decreased by decreasing the non-wetting fluid pressure due to gas production. This causes fluids interfaces begin to change gradually and imbibition process starts.

5- With known initial water saturation, A_w and r_w can be calculated for each element by Eqs. (5) and (7), respectively.

6- As the pressure gradient in non-wet fluid (gas) is ignored and gas pressure is constant in the pore network, the wet phase pressure in all elements is calculated by Eq. (29) using known capillary pressure.

7- Pore threshold capillary pressure is calculated by Eq. (11). Throat threshold capillary pressure for frontal displacement and snap-off are calculated by Eq. (9) and (10), respectively. There is a competition between these displacement events in throats. The mechanism yielding greater threshold pressure is dominated for the corresponding throat.

8- Elements connected to wet front are specified.

9- Threshold pressures of elements are compared so that the element with maximum threshold value is chosen for invasion of wetting-phase and its threshold pressure is set equal to current capillary pressure of the network.

10- Δt is calculated for the invaded element by Eq. (30).

11- Knowing $r_{w/nw}$, the saturation at time step of n+1, $S_{w,i}^{n+1}$ is calculated by Eq. (8) and Eq. (29) is used for all the elements (pores and throats) of the pore network that forms a set of nonlinear equations that updates P_w for all elements.

12- Elements capillary pressures are updated.

13- After filling each element P_w, r_w , A_w and finally S_w are updated.

14- Procedure is repeated from step 11. The simulation stops when interfaces are not moving any more.

RESULTS AND DISCUSSION

The described 2D pore network modelling for dynamic displacement should be validated. To do this a network with identical pore and throat radius sizes is considered

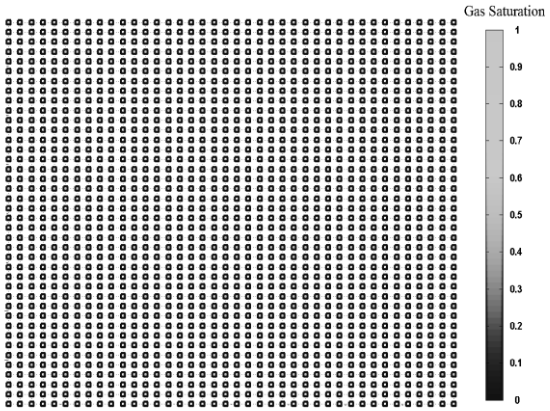

Fig. 6: Network model after water imbibition.

and a piston-wise displacement of gas by water is observed so that no residual gas saturation remains in the network as it is shown in Fig. 6. This result confirms the validity of the modelling method,

The modelling method is used to study the effect of the pore and throat size, pore shape, aspect ratio, coordination number and capillary number on the amount of residual gas saturation in water imbibition. The results are compared to the results of micromodel experiments and the experimental results are generalized using pore network simulations.

To study the effect of the pore and throat size on the mechanism of imbibition, two micromodels No. 1 and 3 are chosen from Table 1 that have identical pore and throat shapes (square cross section) and approximately similar aspect ratio but different sizes of pores and throats.

To compute above results, basic network model result is compared with the results of pore networks with identical aspect ratio but smaller minimum and maximum pore radii. Pore size distribution function of these networks is shown in Fig. 7. RGS are compared for these pore network structures in Fig. 8.

According to Figure 8, same trend of decreasing RGS with increasing pore sizes is observed with pore network modelling and micromodel experiments. Increase in pore radii decreases threshold capillary pressures, which lead to decrease snap-off occurrences.

To examine the effect of the shape of pores cross section areas on imbibition process, the experimental results of micromodels No.1 and No.2 are compared with

Table 3: Comparison of micromodel results for investigating the effect of the pore size.

Micromodel No.	S_{wi}	S_{gr}
1	0.18	0.1
3	0.27	0.21

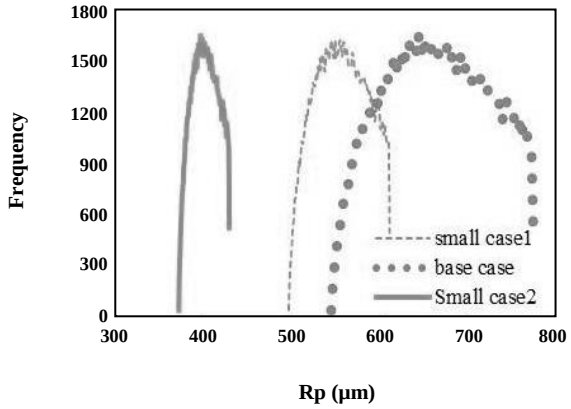

Fig. 7: PDF of networks with different pore and throat radius.

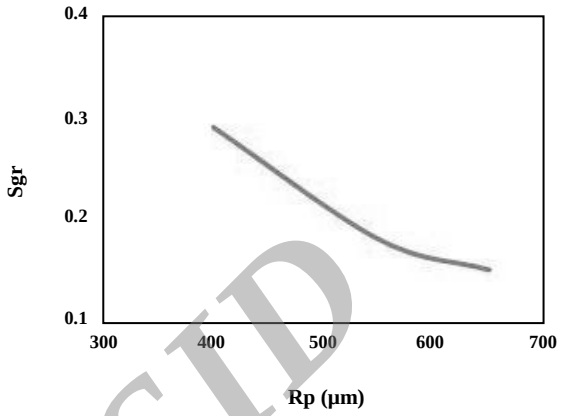

Fig. 8: S_{gr} in pore networks with different pore and throat radius.

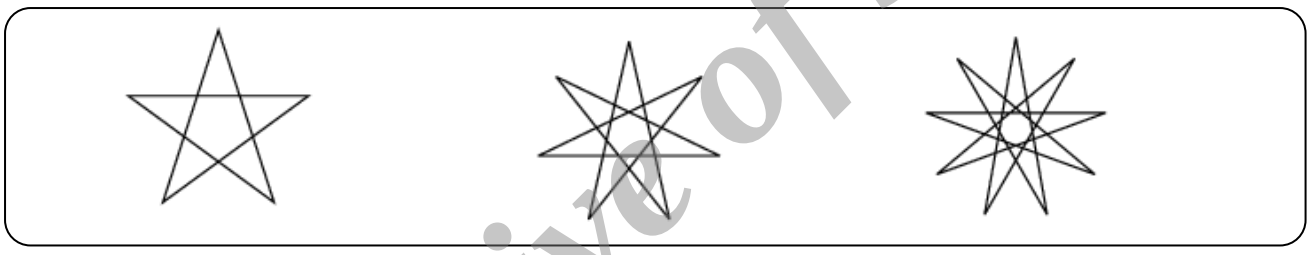

Fig. 9: Star shape pore cross section (A) 5/2 star, (B) 7/3 star and (c) 9/5 star.

each other that have pores shapes of square and star cross sections area, respectively and nearly the same aspect ratio. Comparison of the results shows that increasing the angularity (decrease half angle) causes an increase in initial water saturation from 0.18 to 0.32 and an increase in residual gas saturation from 0.1 to 0.28.

To confirm above experimental results, the results of RGS for the basic pore network model with square cross section are compared to those of networks with regular star shaped cross sections consisting of different number of points, as shown in Fig. 9.

According to Fig. 10, by increasing the number of points in star shaped pores cross section area the corners' angle (α) get smaller. Equations (9) and (10) show that decrease in α results higher $P_{c,thS}$ compared to $P_{c,t}$ and causes an increase in the number of snap-off events and RGS.

It should be noted that coordination number differs in these two micromodels. To study the effect of coordination number on RGS, by some of the throats are randomly removed from the 2D pore network to construct networks with <Z><4. The fraction of removed pores p can be calculated by:

$$p = 1 - \frac{\langle Z \rangle}{4} \tag{28}$$

In a real pore space, connectivity is not identical in all the pores due to the heterogeneity of pore space. RGS for networks with different coordination numbers are compared in Fig. 11.

As Fig. 11 shows, by decreasing the coordination numbers or increasing the fraction of removed pores or increasing the heterogeneity of the pore space RGS is increased. Since throat sizes are generally smaller than pores and some of them are removed to increase heterogeneity, thus in drainage process water that remains in smaller zones will be less and initial water saturation

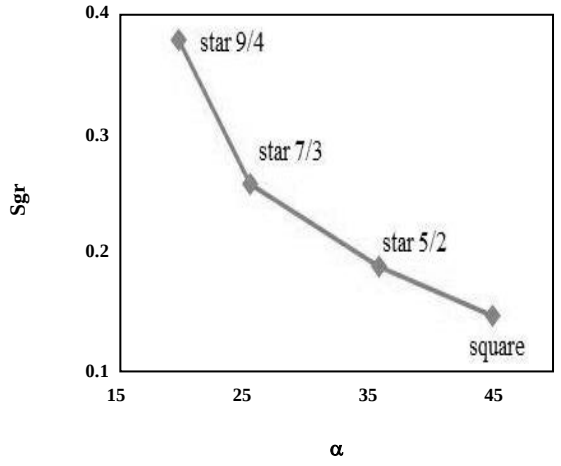

Fig. 10: Effect of pore shape on S_{gr}.

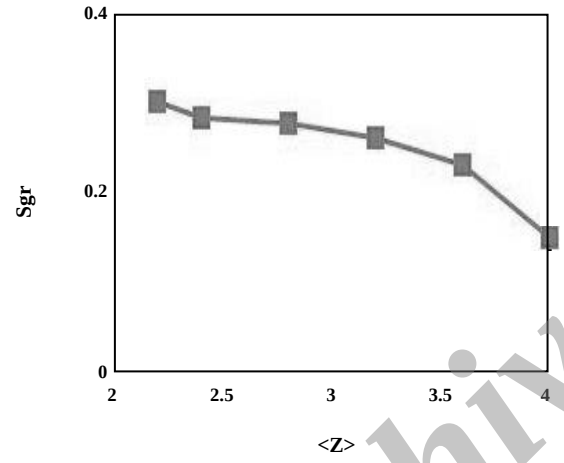

Fig. 11: Effect of coordination number on S_{gr}.

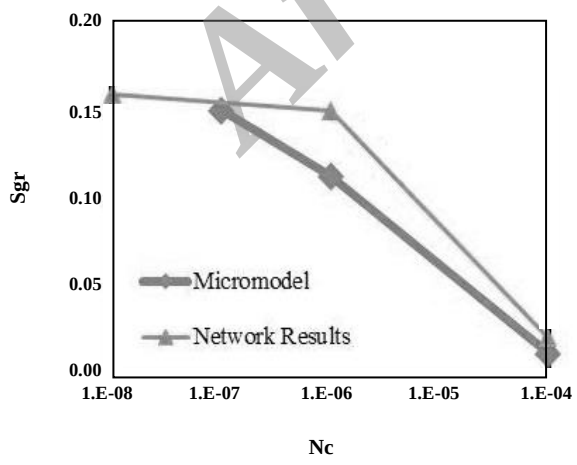

Fig. 12: Effect of the N_c on S_{gr}.

will decrease. However, imbibition starts from the smaller elements that have higher threshold capillary pressure. In a heterogeneous network the water film pressure in throats increases and causes higher occurrences of snap-off events and RGS.

To study the effect of water flow rate on RGS, different water flow rates are injected to micromodel No.1. Hence, a constant gas pressure is set (15 psig) at the micromodel outlet by using a back pressure regulator and one pore volume water is injected to the micromodel inlet at different flow rates. The results show that RGS is decreased by increasing water injection flow rate. The variation of RGS with N_c for the aspect ratio of 2.31 is compared with micromodel results in Fig. 12. N_c is also reported which is calculated as follows,

$$N_c = \frac{\mu v}{\sigma} \tag{29}$$

It shows that RGS does not change significantly until N_c reaches 10^{-7} where viscous force is low and capillary force is dominant because the flow rate is very low. Thus the imbibition mechanism is spontaneous indicating that the critical capillary number in gas-water displacement is around 10^{-7} which is smaller than the critical capillary number for mobilizing the residual oil in oil-water displacement that is about 10^{-5} [27]. Comparing calculated RGS of network model with the measured one in micromodel experiments minimum error exist in low capillary numbers.

These results also suggest that RGS is not only a function of petrophysical property and pore morphology, but also it depends on flow rate and the experimental procedure.

CONCLUSIONS

In this study a micromodel set-up is designed to provide an experimental tool for observing two phase water/gas flow in porous media and determine important parameters in RGS in pore scale. These results are compared with network model results. According to the results pore morphology has an important effect on the RGS. Increasing the pore and throat size decreases RGS. Pore shape and shape half angle affects RGS. Increasing angularity that results in decreasing in half angle lead to RGS increase. Also, increasing porous media heterogeneity with decreasing coordination number causes an increase

in RGS. The results also indicate that RGS is not only a function of petrophysical property and pore morphology, but also it depends on flow rate and the experimental procedure. RGS does not change significantly when N_c is less than 10^{-7}. Comparison of the experimental results of micromodels with simulated pore network model results shows that these results are closer to each other in lower capillary numbers when the effect of the viscous forces is lower in micromodel experiments.

Received : May 4, 2014 ; Accepted : Apr. 13, 2015

REFERENCES

[1] Geffen T., Parrish D., Haynes G., Morse R., Efficiency of Gas Displacement from Porous Media by Liquid Flooding, *Journal of Petroleum Technology*, **4**: 29-38 (1952).

[2] Land C., Comparison of calculated with experimental imbibition relative permeability, *Old SPE Journal*, **11**: 419-425 (1971).

[3] Kleppe J., Delaplace P., Lenormand R., Hamon G., Chaput E., Representation of Capillary Pressure Hysteresis in Reservoir Simulation, *SPE 38899*, "Proceedings of the SPE Annual Meeting", San Antonio, Texas, (1997).

[4] Suzanne K., Hamon G., Billiotte J., Trocme V., Distribution of Trapped Gas Saturation in Heterogeneous Sandstone Reservoirs, " Proceedings of the Annual Symposium of the Society of Core Analysts", Abu Dhabi, (2001).

[5] Chierici GL and Ciucci GM, Water Drive Gas Reservoirs: Uncertainty in Reserves Evaluation from Past History, *Journal of Petroleum Technology*, **19** (2): 237-44 (1967).

[6] Hamon G., Suzanne K., Billiotte J., Trocme V., Field-Wide Variations of Trapped Gas Saturation in Heterogeneous Sandstone Reservoirs, "In SPE Annual Technical Conference and Exhibition", Louisiana, (2001).

[7] Delclaud J., Laboratory Measurements of the Residual Gas Saturation, In: "Advances in Core Evaluation II: Reservoir Appraisal: Reviewed Proceedings of the Second Society of Core Analysts European Core Analysis Symposium", **2**: 431-451 (1991).

[8] McKay B., Laboratory Studies of Gas Displacement from Sandstone Reservoirs Having Strong Water Drive, *APEA Journal*, **189**: 189-194 (1974).

[9] Crowell D. C., Dean G., Loomis A., "Efficiency of Gas Displacement from a Water-Drive Reservoir", US Dept. of the Interior, Bureau of Mines, **6735** (1966).

[10] Bull Ø., Bratteli F., Ringen J. K. , Melhuus K., Bye A.L., Iversen J. E. , The Quest for the True Residual Gas Saturation–an Experimental Approach, "International Symposium of the Society of Core Analysts", Texas, USA, p. 1-12, (2011).

[11] Lenormand R., Liquids in Porous Media, *Journal of Physics: Condensed Matter*, **2**: SA79 (1999).

[12] Blunt M. J., Scher H., Pore-level Modeling of Wetting, *Physical Review E*, **52**: 6387 (1995).

[13] Mogensen K., Stenby E. H., A Dynamic Two-Phase Pore-Scale Model of Imbibition, *Transport in Porous Media*, **32**: 299-327 (1998).

[14] Hughes R.G. Blunt M.J., Pore Scale Modeling of Rate Effects in Imbibition, *Transport in Porous Media*, **40**: 295-322, (2000).

[15] Hekmatzadeh M., Dadvar M., Emadi M., Pore Network Modeling for Prediction of Residual Gas Saturation in Water Invasion Process, *J. of Porous Media*, **17**: 503-520 (2014).

[16] Jamshidi S., Bozorgmehry R., Pishvaie M., An Irregular Lattice Pore Network Model Construction Algorithm, *Iran. J. Chem. Chem. Eng. (IJCCE)*, **29**(1): 61-70, (2010).

[17] Coxeter H. S. M., "Introduction to Geometry", John Wiley & Sons, 36-38 (1961).

[18] Piri M., Blunt M.J., Three-Dimensional Mixed-Wet Random Pore-Scale Network Modeling of Two- and Three-Phase Flow in Porous Media. II. Results, *Phys. Rev., E*., **71**: 026331 (2005b).

[19] Al-Gharbi M. S., Blunt M.J., Dynamic Network Modeling of Two-Phase Drainage in Porous Media, *Physical Review E*, **71**: 016308 (2005).

[20] Bernadiner M. G., A Capillary Microstructure of the Wetting Front, *Transport in Porous media*, **30**: 251-265 (1998).

[21] Lenormand R., Zarcone C., Sarr A., Mechanisms of the Displacement of One Fluid by Another in a Network of Capillary Ducts, *J. Fluid Mech*, **135**: 337-353 (1983).

[22] Vizika O. and Payatakes A., Parametric Experimental Study of Forced Imbibition in Porous Media, *Physico Chem. Hydro Dyn*, **11**: 187-204 (1989).

[23] Oren P.E., Bakke S., Arntzen O.J., Extending Predictive Capabilities to Network Models, *SPE Journal*, **3**: 324-336 (1998).

[24] Patzek T., Verification of a Complete Pore Network Simulator of Drainage and Imbibition, *SPE Journal*, **6**: 144-156 (2001).

[25] Ransohoff T., Radke C., Laminar Flow of a Wetting Liquid Along the Corners of a Predominantly Gas-Occupied Noncircular Pore, *J. Colloid Interface Sci*., **121**: 392-401, (1988).

[26] Zhou D., Blunt M. J., Orr F. M., Hydrocarbon Drainage Along Corners of Noncircular Capillaries , *J. Colloid Interface Sci*., **187(1)**: 11-21..0. (1997).

[27] Chatzis I., Morrow N., Measurement and Conditions for Entrapment and Mobilization of Residual, *US DOE Final Report*, **DOE/BETC/3251-12** (1981).